Energy Conversion and Management 64 (2012) 397–402

Contents lists available at SciVerse ScienceDirect

Energy Conversion and Management

journal homepage: www.elsevier.com/locate/enconman

Thermoelectric energy harvesting from diurnal heat flow in the upper soil layer

Scott A. Whalen [a,*], Ronald C. Dykhuizen [b]

[a] Pacific Northwest National Laboratory, 902 Battelle Blvd., Richland, WA 99352, United States
[b] Sandia National Laboratories, 1515 Eubank Blvd., SE, Albuquerque, NM 87185-6972, United States

ARTICLE INFO

Article history:
Received 3 November 2011
Received in revised form 6 June 2012
Accepted 15 June 2012
Available online 27 September 2012

Keywords:
Thermoelectric
Energy harvesting
Soil
Subterranean
Thermopile
Solar

ABSTRACT

We built and tested a subterranean thermoelectric power source that converts diurnal heat flow through the upper soil layer into electricity. This paper describes the operation, design, and performance of the device. Key features of the power source include the use of bismuth-telluride thermopiles optimized for small ΔT and aerogel insulation to minimize thermal losses. The device weighs 0.24 kg and was designed with a flat form factor measuring $12 \times 12 \times 1.7$ cm to facilitate modularity, packing, and assembly into larger arrays. One full year of field testing was performed between June 2009 and May 2010 in Albuquerque, New Mexico where the device generated an average power output of 1.1 mW. The season with the highest performance was spring (March–May) while the season of lowest performance was winter (November–January). During May 2010, the device generated an average power of 1.5 mW and a peak power of 9.8 mW at 9.3 V. Ten years of continuous operation at 1.1 mW would yield an energy density and specific energy of 1384 W h/L and 1430 W h/kg respectively, which is competitive with chemical batteries and is orders of magnitude greater than published subterranean and ambient thermoelectric harvesters. Numerical simulations show that performance is sensitive to the thermal properties of the soil and environmental conditions. This class of energy harvester may provide an option for supplemental power, or possibly primary power, for low power remote sensing applications.

1. Introduction

Chemical batteries are the power source of choice for many unattended ground sensor systems [1,2] due to their maturity, low cost, ruggedness, and reliability. A drawback to batteries in these applications is that replacement or recharging may not be feasible because access to remote sensors after deployment can be challenging or impossible. A popular approach to extending battery life is using commercially available solar cells to provide supplemental power [3–5]. However, there are situations where the use of solar cells is not feasible. An alternative to solar power is the use of thermoelectric energy harvesters that convert environmental temperature differences into electricity. Although ambient thermoelectric power sources have not yet realized commercial use due to low conversion efficiencies compared to solar cells [6,7], there are circumstances where thermoelectric harvesters offer a unique solution when batteries or solar cells are not operationally feasible. In this paper we propose a subterranean thermoelectric harvester driven by diurnal temperature fluctuations in the upper soil layer.

The basic architecture of a subterranean harvester consists of thermoelectric modules (thermopiles) attached to hot and cold plates that are separated by thermal insulation. Diurnal temperature fluctuations in the environment induce thermal gradients in the soil which are converted into electricity. Since diurnal heat fluxes are small within the upper soil layer (2–15 mW/cm^2 during the day) [8], the temperature differences (ΔT) that can be developed across a thermopile are also small. It is critical that the power source is designed to maximize ΔT across the thermopiles given that thermoelectric conversion efficiency is dependent on ΔT [9]. Thermal losses between the hot and cold plates should be minimized using low conductance insulation and the geometry of the thermopile and plates must be optimized for maximum efficiency [10]. It is important to determine the expected soil characteristics [11], soil interaction with the plates [12], and thermal conductance of the thermopile [13] in order to optimize performance. Literature also emphasizes that the depth of the lower heat plate can be designed to maximize ΔT [14]. In addition to subterranean operation, similar design principles could be applied to energy harvesting at the air/water interface in aquatic environments [15].

A few examples of subterranean thermoelectric harvesters do appear in the literature. Calculations for one device indicate a peak power output on the order of 0.40 mW [16] while another device

* Corresponding author. Tel.: +1 509 372 6084; fax: +1 509 372 4353.
E-mail address: scottwhalen@asme.org (S.A. Whalen).

0196-8904/$ - see front matter © 2012 Elsevier Ltd. All rights reserved.
http://dx.doi.org/10.1016/j.enconman.2012.06.015

generated a peak of 0.10 mW at 100 mV [17]. Power output was limited in both of these devices because the thermopile and insulation were not optimized. There is a body of work in the literature showing that subterranean harvesters have achieved a peak power near 10 mW at battery-like voltages [18,19] and an average power output in the milliwatt range [20]. High-aspect ratio thermoelectric elements are the key to maximizing conversion efficiency from small temperature differences while generating a battery-like voltage. Optimized thermopiles, used in [20], have been fabricated containing thousands of elements exceeding 1 cm in length with leg widths less than 100 μm [21]. Thermopiles designed for use in cooling applications have also been evaluated for autonomous power [22]. This study shows that large heat fluxes, on the order of 1000 mW/cm^2, are required to generate 2 V because the element aspect ratio is not optimized for small ΔT. Such large heat fluxes are not to be found in the upper soil layer. The objective of our work was to design, model, and test a subterranean thermoelectric harvester that is optimized for small ΔT operation and maximizes energy density and specific energy. The harvester was initially characterized in a laboratory setting and subsequently tested for one full year in a field environment. Experimental results are compared with simulations, batteries, and thermoelectric ambient energy harvesters from the literature.

2. Operation

The earth's surface temperature increases as solar heat penetrates the upper soil layer throughout the morning hours. A positive voltage is generated during this time as a thermal gradient develops across the buried power source. The largest heat flow and temperature difference occur near midday resulting in the maximum voltage and power output. The thermal gradient decreases in the upper soil layer throughout the afternoon hours and eventually reverses during the early evening as heat is rejected to the atmosphere. During this time, the voltage output decreases until the polarity reverses. The largest nighttime heat flow and temperature difference occur near midnight resulting in the maximum negative voltage. Excellent diagrams of the day and night heat exchange processes in the upper soil layer are shown in [23]. A subterranean thermoelectric harvester exploits the oscillating heat flux within the upper soil layer.

3. Design and fabrication

Fig. 1 shows a schematic cross-section of a unit cell during daytime operation (not to scale). The device consists of five key components: a hot side plate, thermopile, cold side plate, thermal insulation, and an environmental barrier. Four unit cells were assembled into an array to build a thermoelectric power source (TPS) assembly. The TPS is designed to generate single-digit milliwatts at a battery-like voltage while minimizing weight and volume. Each unit cell has an optimum cross sectional area of 6×6 cm that maximizes power density. As such, the hot and cold plates of the four-cell TPS measure 12×12 cm. The resulting TPS geometry has a relatively flat form factor and does not rely on exchanging heat with the constant temperature soil depth.

Bismuth-Telluride (Bi_2Te_3) was chosen as the thermoelectric material for its superior conversion efficiency in the expected temperature range compared to other bulk materials. The thermoelectric element geometry and number of couples was optimized for maximum efficiency when $\Delta T = 20$ °C and $V_{load} = 10.6$ V with the four thermopiles connected in series. Each thermopile contains 1296 elements (630 couples) each measuring $0.30 \times 0.30 \times 13$ mm. This high-aspect ratio ($L/A = 144$ [1/mm]) is critical to maximizing conversion efficiency when the available heat flux is small and battery-like voltage is required. We note that the number of couples is slightly less than half the number of elements due to a wiring scheme devised to aid fabrication. The elements are bonded together into a robust monolithic array, as seen in Fig. 2, using a polymer binder whose width is kept to a minimum to reduce parasitic thermal losses. Elements within each thermopile are connected in series using electroplated metallic contacts.

Anodized 6061-T6 aluminum was chosen as the plate material for its corrosion resistance and high thermal conductivity to density ratio (0.84 for 6061-T6 compared to .45 for Cu and 0.53 for Mg AZ31B). The thermopiles are mechanically robust and act as structural members between the heat plates which means the thermal insulation is not required to be load bearing. As a result, Aerogel filled with silica and titania powder was chosen as the insulation material for its low thermal conductivity (0.012 W/m K at STP) and density (0.24 g/cm^3). A low thermal conductivity insulator is critical for concentrating heat flow through the thermo-

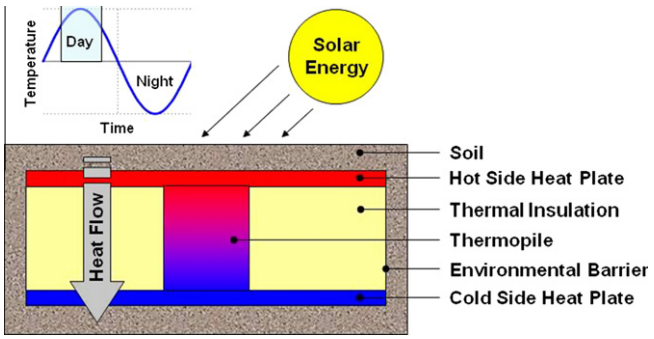

Fig. 1. Unit cell schematic.

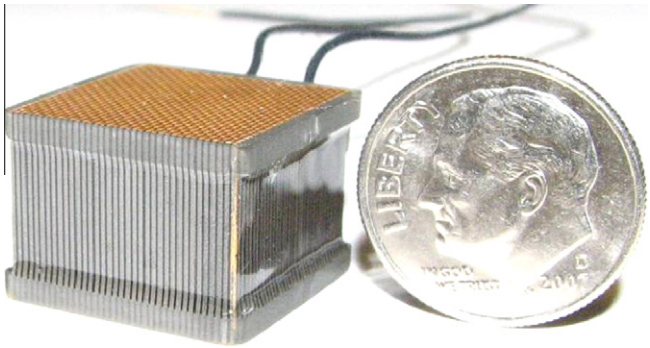

Fig. 2. Monolithic Bi_2Te_3 thermopile.

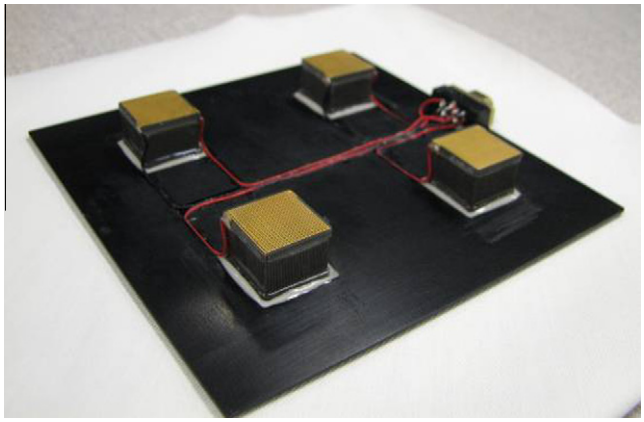

Fig. 3. Thermopiles bonded to the heat plate.

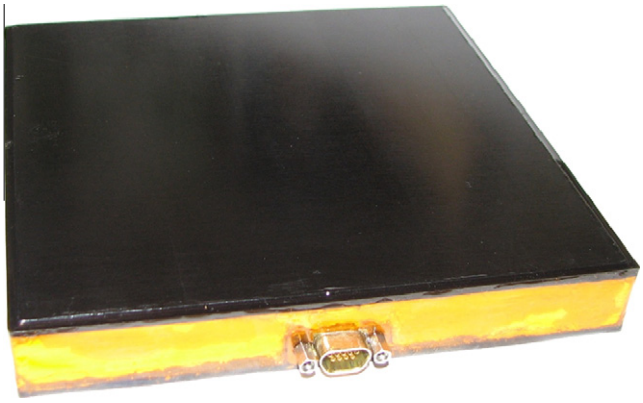

Fig. 4. Assembled TPS.

piles. The TPS is assembled by first bonding four thermopiles to the heat plate using ceramic filled epoxy. Ceramic filler reduces the thermal drop across the interface bond without shorting the exposed electrical contacts. Fig. 3 shows the bonded thermopiles with wires routed to a connector. The thermopiles can be wired in a series or parallel combination to build either current or voltage. An aerogel insulator is placed within this assembly, the thermopiles are coated with ceramic filled epoxy, and the second heat plate is attached. The perimeter of the TPS is wrapped with a 5 mil thick Kapton® film and sealed with epoxy to provide an environmental barrier. Finally, the entire part is baked at 100 °C for 24 h to fully cure the epoxy. The completed TPS (Fig. 4) measures 12 × 12 × 1.7 cm, has a mass and volume of 0.24 kg and 0.25 L respectively, and an internal AC resistance of 6.4 kΩ when the four thermopiles are wired in series.

4. Laboratory testing

We performed laboratory testing to characterize the TPS performance within the range of operating temperatures expected in the field. This included determining the optimum load resistance and measuring open circuit voltage, load voltage, and power output as a function of temperature difference. Fig. 5 shows the power output and load voltage as a function of load resistance with the four thermopiles connected in series. A constant $\Delta T = 20$ °C ($T_H = 40$ °C and $T_C = 20$ °C) was imposed across the device in this test while the load resistance varied from 1 Ω to 100 kΩ. Sufficient time was allowed between each electrical load for the TPS to reach thermal equilibrium. The data shows that a load resistance of 8.4 kΩ maximizes power output for $\Delta T = 20$ °C. Type K thermocouples were used to measure the hot and cold side temperatures. The

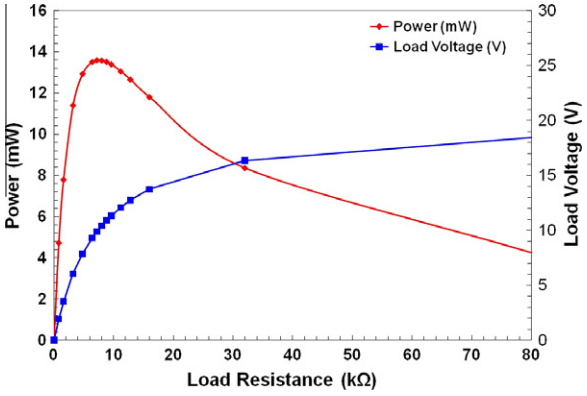

Fig. 5. Optimum load resistance.

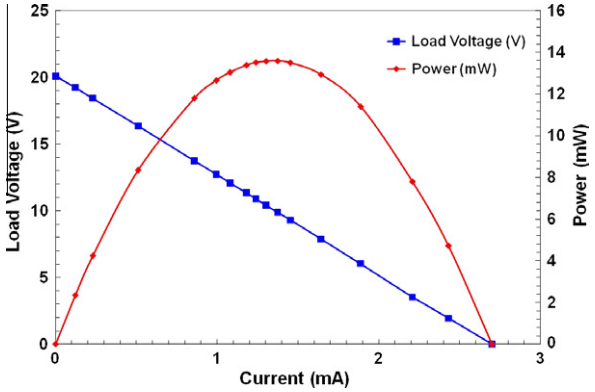

Fig. 6. Power curve.

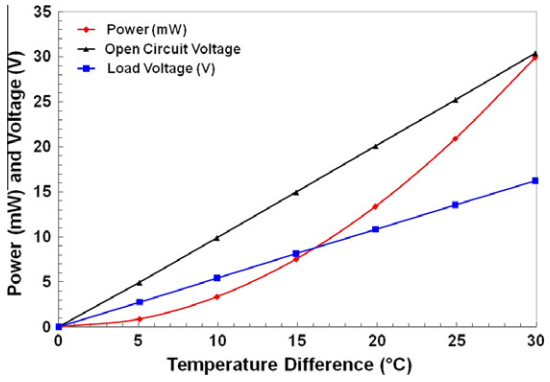

Fig. 7. Electrical performance as a function of ΔT.

thermocouples were individually calibrated against a NIST traceable special platinum resistance thermometer having an accuracy of ±0.010 °C which resulted in a thermocouple uncertainty of ±0.5 °C (±1 °C on ΔT). Voltage was measured using an HP 3457A multi-meter with an accuracy of ±0.002 V. Fig. 6 shows a power curve for the TPS when $\Delta T = 20$ °C ($T_H = 40$ °C and $T_C = 20$ °C). At the optimum load of 8.4 kΩ (±8.4 Ω), the load voltage is 10.6 V and the power dissipated across the resistor is 13.4 mW (±0.014 mW). Fig. 7 shows open circuit voltage, power output, and load voltage as a function of ΔT for a fixed 8.4 kΩ load resistance. The cold side was held constant at 20 °C and the hot side was raised in 5 °C increments to 50 °C. This data shows that battery-like voltages can be developed from small temperature differences. The loaded and open circuit voltages are 5.4 and 9.9 V respectively when $\Delta T = 10$ °C. Very little heat is required (critical to ambient thermal energy harvesting) to generate $\Delta T = 10$ °C due to the optimized thermoelectric element geometry and low thermal conductivity aerogel insulation. Calculations indicate that a heat flux of just 5.3 mW/cm^2 is necessary to generate $\Delta T = 10$ °C. The TPS efficiency is 0.45% when $\Delta T = 10$ °C based on a calculated heat input of 0.76 W and measured power output of 3.4 mW.

5. Field testing

After laboratory characterization, the TPS was moved to an outdoor facility for continuous testing in a field environment on Kirtland Air Force Base. A nearby weather station recorded hourly air temperature, wind speed, and cloud conditions which were subsequently used as inputs to our model for simulating the field tests. The unit was buried under approximately 1 cm of indigenous soil and Fig. 8 shows data for load voltage and power output of the TPS during May 2010. The value on the *x*-axis describes the end of

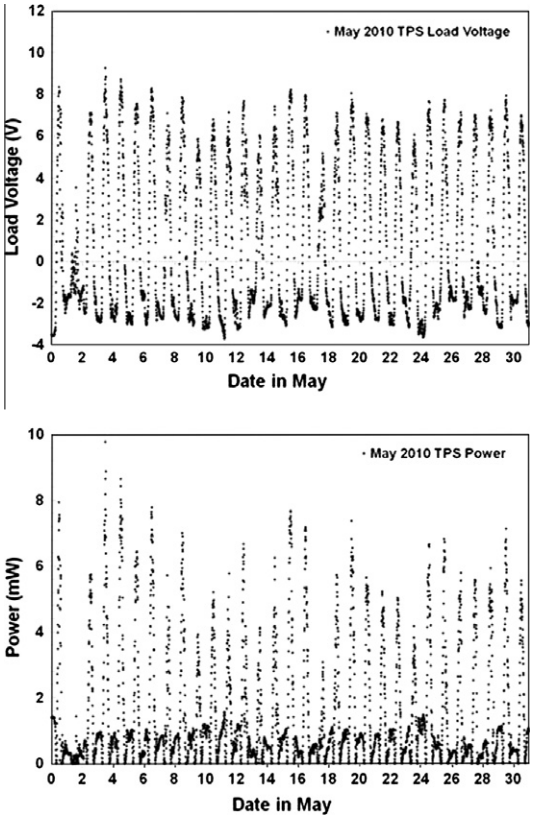

Fig. 8. Load voltage and power output during May 2010.

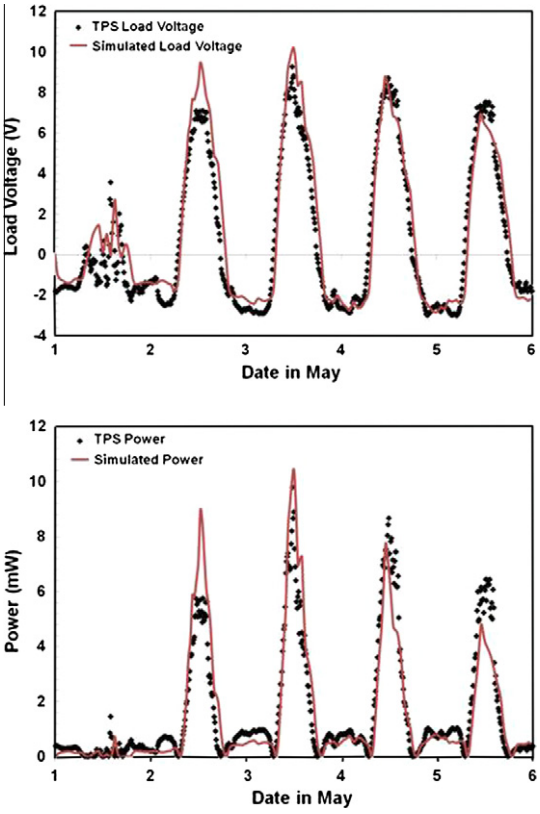

Fig. 10. Measured and simulated electrical output for May 2–6, 2010.

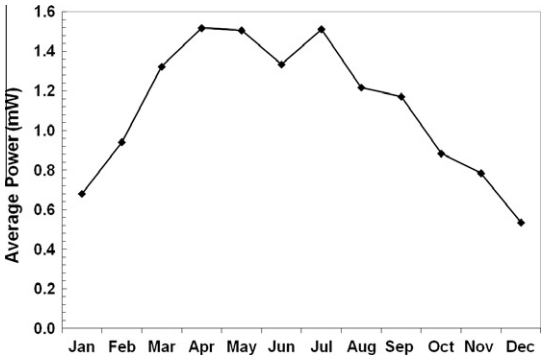

Fig. 9. Monthly power output from June 2009 to May 2010.

the indicated day of the month. Power output is simply calculated as $P = V_{load}^2/8400\,\Omega$ and does not account for inefficiencies that would be present with power management circuitry. The effect of the diurnal temperature cycle is clearly seen as the load voltage oscillates between positive and negative values. The peak day/night voltage averaged 7.2 and −2.8 V for the month, while the peak day/night power averaged 6.0 and 1.1 mW. Averaging the power over the entire month gives a mean output of 1.5 mW. The peaks occurred at midday and midnight and zero output occurred at 4:00 pm and 5:00 am. An analysis of the data shows that 18% of the total power is generated between 4:00 pm and 5:00 am when the voltage output is negative. Fig. 9 shows the average power output by month with the season of highest performance generally occurring in the spring (March–May) because the diurnal temperature fluctuations are the largest during this time. On a yearly basis, the TPS generates an average power output of 1.1 mW.

6. Modeling and parameter variations

We used a simple one-dimensional finite difference conduction model to predict transient temperatures within the TPS and surrounding geologic media. Basic heat transfer analyses with the incorporation of thermoelectric ambient energy harvesters have been adequately described elsewhere [8,13,18,19,24,25] and will not be elaborated here. Generally speaking though, the domain consists of five layers including the soil covering, upper heat plate, thermopile/insulation, lower heat plate, and underlying soil. We utilized an adiabatic boundary condition at a depth of five meters to approximate the constant temperature geologic boundary condition of the soil. Environmental boundary conditions above ground were determined via data from the nearby weather station and estimates for solar flux were based on a simple correlation to account for cloud conditions (clear was 100% solar flux, scattered clouds 90%, partly cloudy 80%, mostly cloudy 50%, overcast 30%, and light rain 10%). Of interest to the reader may be the calculated thermal resistance of the TPS in the open circuit condition. The thermal resistance of R_{th} = 13 K/W for the overall device is quite high given the low aspect ratio (L/A = 0.012 cm^{-1}) and is required for generating large temperature differences from the small diurnal heat flux in the upper soil layer. The thermal resistance of a single thermopile is 60 K/W and four thermopiles in parallel have a value of 15 K/W. The aerogel insulation has a thermal resistance of 103 K/W. The effective thermal conductivity of the TPS is remarkably low at just 0.10 W/mK. This value is similar to that of common materials such as rubber, wood, and leather. In the open circuit condition, approximately 87% of the heat flows through the four thermopiles while just 13% flows through the aerogel insulation. This highlights the effect of the low thermal conductivity insulation given that it occupies 93% of the cross sectional area.

Table 1
Simulations of surface coverings and bulk soil conditions in July 2010.

Case	Peak power (mW)	Covering	Bulk soil
Baseline	7.0	1 cm dry sand	Dry sand
1	12.5	1 cm compact soil	Compact soil
2	16.5	1 cm asphalt	Dry sand
3	25.2	1 cm asphalt	Compact soil
4	11.4	5 cm asphalt	Dry sand
5	17.5	5 cm asphalt	Compact soil

Table 2
Soil properties used in simulations.

Property	Dry sand	Compact soil	Asphalt
ρ (kg/m^3)	1515	2000	2100
Cp (J/kg K)	800	1800	900
k (W/m K)	0.27	0.60	1.0
Emissivity	0.50	0.75	0.95

Accurate simulation results require a stable initial condition to build in the correct temperature gradients within the device and the underlying soil. We chose to start our simulation using environmental data from May 2, 2010 since that day consisted of heavy overcast and light rain. This allowed our simulation to establish a fairly benign initial condition for simulating the following days. Fig. 10 begins at 12:01 am on May 2 and ends at 11:59 pm on May 6 and shows that our simulation results agree well with our measured voltage and electrical power. We over-predict the peak power on May 3, and under-predict the peak power on May 6. The discrepancy in amplitude is likely because the local weather (most likely the cloud conditions) at the test site did not agree with that recorded at the nearby weather station. The soil thermal conductivity may be an additional source of uncertainty since we did not measure the actual soil properties. We used a thermal conductivity of 0.27 W/m K for sand [26] which is comparable to values presented for arid soils [27–29]. Nevertheless, the model appears to closely predict the shape and timing of the data.

We determined through experimentation and numerical simulation that TPS performance is sensitive to the type of covering and underlying soil properties. Our simulations show that increasing the soil conductivity improves power output because more heat flows through the device. This would be representative of soil found in more temperate climates. We also show that power increases as the thickness of the soil covering decreases. An experiment showed that peak power doubled in July, 2010 when the 1 cm soil covering was replaced by a thin dusting. Our numerical model was used to simulate the effects of different covering and underlying soil properties. Table 1 shows the results from these simulations. In general, it is thermal conductivity that varies most between the different cases. It is important to note that material properties for dry sand, compact soil and asphalt vary significantly in the literature. For example, the thermal conductivity of asphalt can vary from 0.8 to 2.8 W/m K [30] while that of dry sand can vary from 0.2 to 1.6 W/m K [27]. Table 2 shows the nominal values used in our simulations. Asphalt has been evaluated for thermal energy harvesting applications [31] and was chosen as a representative covering for installing the TPS in a robust manner such as within a paved road.

Table 1 shows that peak power increases as the thermal conductivity of the covering and/or the underlayment increases from dry sand, to compact soil, to asphalt. The power level is shown to be significant even when the thickness of the asphalt covering is increased from 1 to 5 cm. We also examined using four copper spikes measuring 1 cm in diameter and 20 cm long to heat sink the TPS to cooler soil. Using copper spikes resulted in an improvement of 85 percent in power compared to the baseline prototype; however, this approach adds 0.56 kg and 0.063 L to the TPS. Combining case 3 with copper spikes increased peak power by nearly a factor of 7 to 46.6 mW.

Table 3
Comparison of primary batteries with the TPS at 10 years.

Technology	W h/L	W h/kg
TPS baseline	387	400
Case 1	692	715
Case 2	900	930
Case 3	1384	1430
Case 3 w/spikes	2079	808
$Li/SOCl_2$	1100	590
Li/CF_x	635	250
Zn–Air	1300	370

Table 4
Comparison of thermoelectric ambient energy harvesters with the TPS at 10 years.

Technology	W h/L	W h/kg
TPS Case 3	1384	1430
Device 1 [33]	259	N/A
Device 2 [18,20]	58	52
Device 3 [17]	12	2
Device 4 [16]	1	1

7. Comparisons

Table 3 gives a comparison of TPS energy density and specific energy at 10 years with that of four primary battery chemistries [32]. This comparison does not account for degradation in battery performance due to thermal cycling, temperature extremes, or self-discharge nor does it consider inefficiencies in power management circuitry required for the TPS. The TPS compares favorably with batteries at 10 years in terms of energy density and generally exceed batteries in terms of specific energy. An alternative comparison is made between the TPS and another subterranean power source [18,20]. This comparison device uses Bi_2Te_3 thermoelectric materials, weighs 2.0 kg, and is cylindrical in shape having a diameter of 9.6 cm, length of 25 cm, and volume of 1.8 L. The cross sectional area of this device is half that of the TPS and the length is approximately 15 times greater. The power output is given as 1.2 mW and includes power management circuitry. Although the specific burial conditions (depth and soil type) are not specified, it appears that our baseline TPS generates a similar average power output (1.1 mW) with a significantly lower mass and volume (0.24 kg and 0.25 L compared to 2.0 kg and 1.8 L). Table 4 compares the energy density and specific energy of the TPS with ambient energy thermoelectric harvesters found in the literature. Values were calculated to the best of our ability from the data reported in the literature. Performance of the TPS exceeds that of the comparison devices by orders of magnitude in some cases. The high energy and power densities are primarily due to the thermopiles being optimized for small ΔT and use of aerogel insulation to minimize parasitic thermal losses.

8. Conclusions

Milliwatts of continuous power at battery-like voltages can be harvested from diurnal variations in heat flow through the upper soil layer. This is possible in a flat form factor that does not rely on exchanging heat with the constant temperature soil depth. Numerical simulations have shown that performance is sensitive to thermal history, environmental conditions, and thermal properties of the covering and underlying soil. Ten years of continuous

operation at 1.1 mW would yield an energy density and specific energy of 1384 W h/L and 1430 W h/kg respectively, which is competitive with chemical batteries and is orders of magnitude greater than published subterranean harvesters. This type of energy harvester may provide a power source alternative for long-term, low power, applications where the use of primary batteries or solar cells is not feasible.

Acknowledgements

The authors thank Josh Moczygemba at Marlow Industries, Inc. and Steven Jones at The Jet Propulsion Laboratory for their excellent technical input and fabrication of our custom thermopile and aerogel designs. We also thank the numerous reviewers of this work for their thoughtful input.

Sandia National Laboratories is a multi-program laboratory managed and operated by Sandia Corporation, a wholly owned subsidiary of Lockheed Martin Corporation, for the United States Department of Energy's National Nuclear Security Administration under Contract DE-AC04-94AL85000.

References

[1] Jones B. A roadmap to truly disposable unattended ground sensor (UGS) systems. In: Conference on unattended ground, sea, and air sensor technologies and applications XII, proceeding of SPIE international society for optical engineering, vol. 7693, Orlando, FL; April 2010.
[2] Craig H. Applications for battery powered CP remote monitoring. Mater Perform 2011;50(5):33–55.
[3] Gibson T, Kelly N. Solar photovoltaic charging of lithium-ion batteries. J Power Sources 2010;195(12):3928–32.
[4] Kelly N, Gibson T. Solar photovoltaic charging of high-voltage nickel metal hydride batteries using DC power conversion. J Power Sources 2011;196(23):10430–41.
[5] Sims P. Solar battery recharge options for unattended ground sensors. In: Conference on unattended ground sensor technologies and applications III, proceeding of SPIE international society for optical engineering, vol. 4393, Orlando, FL; April 2001.
[6] Chen J. Thermodynamic analysis of a solar-driven thermoelectric generator. J Appl Phys 1996;79(5):2717–21.
[7] Sodano H, Simmers G, Dereux R, Inman D. Recharging batteries using energy harvested from thermal gradients. J Intell Manuf 2007;18(1):3–10.
[8] Mikityuk P. Thermoelectr Convers Therm Flows Soil. J Thermoelectr 2003(1).
[9] Rowe D. Handbook of thermoelectrics. CRC Press, Inc.; 1995. pp. 24.
[10] Stevens J. Optimized thermal design of small ΔT thermoelectric generators. Energy Convers Manage 2001;42(6):709–20.
[11] Gemant A. The thermal conductivity of soils. J Appl Phys 1950;21(8):750–2.
[12] Henderson J. Analysis of a heat exchanger-thermoelectric generator system. In: Proceedings of the 14th intersociety energy conversion conference, Boston, MA, vol. 2; August 1979. p. 1835–40.
[13] Mikityuk P. Temperature and thermal flow distribution through thermopile in active soil layer. J Thermoelectr 2002(3).
[14] Maixner M, Stevens J. Assessment of near-surface ground temperature profiles for optimal placement of a thermoelectric device. Energy Convers Manage 2000;50:2361–5.
[15] Davidson J, Collins M, Behrens S. Thermal energy harvesting between the air/water interface for powering wireless sensor nodes. Proc SPIE 2009;7288:728814-1–728814-11.
[16] Lawrence E, Snyder G. A study of heat sink performance in air and soil for use in a thermoelectric energy harvesting device. In: 21st ICT, Long Beach, CA; August 2002. pp. 446–9.
[17] Lorenz R. Subsurface ambient thermoelectric power for moles and penetrators. In: IEEE aerospace conference, Big Sky, MT; March 2003.
[18] Anatychuk L, Mikityuk P. Thermal generators using heat flow in soils. In: 22nd International conference on thermoelectrics (ICT), La Grande Motte, France; August 2003. p. 598–601.
[19] Mikityuk P, Petrenko N. Thermoelectric power source using the heat of soil. J Thermoelectr 2003(2).
[20] Institute of Thermoelectricity; 2011. <http://ite.cv.ukrtel.net/>.
[21] Anatychuk L, Demchuk B. Particularly reliable microthermopiles for generators with isotopic heat sources based on ^{238}Pu. In: 22nd ICT, La Grande Motte, France; August 2003. p. 594–7.
[22] Ferrari M, Ferrari V, Guizzetti M, Marioli D, Taroni A. Characterization of thermoelectric modules for powering autonomous sensors. IEEE Trans Instrum Meas 2009;58(1):99–107.
[23] Mikityuk P. Thermoelectric conversion of thermal flows in soil. J Thermoelectr 2003.
[24] Stevens J. Heat transfer and thermoelectric design considerations for a ground source thermoelectric generator. In: 18th ICT, Pardubice, Czech Republic; August, 1999. p. 68–71.
[25] Saqr K, Mansour M, Munsa M. Thermal design of automobile exhaust based thermoelectric generators: objectives and challenges. JAT 2008;9(2):155–60.
[26] Incropera F, Dewitt D. Fundamentals of heat and mass transfer. 3rd ed. New York, NY: John Wiley & Sons; 1990. Appendix A.
[27] Becker E, Fircke B. Effects of saturation and dry density on soil thermal conductivity. In: 3rd International conference on heat pumps in cold climates, Wolfville, Nova Scotia; August 1997. p. 121–36.
[28] Wang K, Wang P, Liu J, Sparrow M, Haginoya S, Zhou Z. Variation of surface albedo and soil thermal parameters with soil moisture content at a semi-desert site on the western Tibetan Plateau. Bound Lay Meteorol 2005;116(1):117–29.
[29] Gao A, Bian L, Hu Y, Wang L, Fan J. Determination of soil temperature in an arid region. J Arid Environ 2007;71:157–68.
[30] Chadbourn, et al., Consideration of Hot-Mix Asphalt Thermal Properties During Compaction, Quality Management of Hot-Mix Asphalt, ASTM STP-1299; 1996.
[31] Mallick R, Chen B, Bhowmick S. Harvesting energy from asphalt pavements and reducing the heat island effect. Int J Sust Eng 2009;2(3):214–28.
[32] Linden D, Reddy T. Handbook of batteries. 3rd ed. New York, NY: McGraw-Hill; 2002. pp. 1.12–1.13.
[33] Knight C, Davidson J. Thermal energy harvesting for wireless sensor nodes with case studies. In: Adv Wireless Sens Netw. Berlin: Springer-Verlag; 2010. p. 221–42.